Reduction-enhanced water flux through layered graphene oxide (GO) membranes stabilized with H_3O^+ and OH- ions

Journal Name

ARTICLE TYPE

Cite this: DOI: 10.1039/xxxxxxxxxx

Reduction-Enhanced Water Flux through Layered Graphene Oxide (GO) Membranes Stabilized with H_3O^+ and OH^- Ions†

Abhijit Gogoi,*[a,c] Erik C. Neyts[a,b] and François M. Peeters[c,d]

Received Date
Accepted Date

DOI: 10.1039/xxxxxxxxxx

www.rsc.org/journalname

Graphene oxide (GO) is one of the most promising candidates for next generation of atomically thin membranes. Nevertheless, one of the major issues for real world application of GO membranes is their undesirable swelling in an aqueous environment. Recently, we demonstrated that generation of H_3O^+ and OH^- ions (e.g., with an external electric field) in the interlayer gallery could impart aqueous stability to the layered GO membranes[1]. This, however, compromises the water flux through the membrane. In this study, we report on reducing the GO nanosheets as a solution to this issue. With the reduction of the GO nanosheets, the water flux through the layered GO membrane initially increases and then decreases again beyond a certain degree of reduction. Here, two key factors are at play. Firstly, the instability of the H-bond network between water molecules and the GO nanosheets, which increases the water flux. Secondly, the pore size reduction in the interlayer gallery of the membranes, which decreases the water flux. We also observe a significant improvement in the salt rejection of the membranes, due to the dissociation of water molecules in the interlayer gallery. In particular, for the case of 10% water dissociation, the water flux through the membranes can be enhanced without altering its selectivity. This is an encouraging observation as it breaks the traditional tradeoff between water flux and salt rejection of a membrane.

1 Introduction

In the past decade, the rapid progress in the development of two dimensional (2D) materials paves the way for the fabrication of thin defect free films consisting of nanometer-thick nanoflakes[2–8]. Some common 2D hydrophilic flakes such as graphene oxide (GO), MXenes contain various functional groups on the surface of the nanosheets which makes them excellent candidates for separation and purification applications[9–14]. Owing to their atomic thickness, mechanical/chemical robustness, high aspect ratio, easy film formation, and tunable structural design, they emerge as perfect contenders for the development of next-generation membranes[15–19].

In particular graphene oxide (GO), a derivative of graphene, has been in focus for membrane applications owing to for example the presence of abundant oxygen containing functional groups, superior water flux, high selectivity, excellent fouling resistance, easy scalability, and high aspect ratio[20–27]. In graphene oxide (GO), the carbon atoms are organised in a tight monolayer honeycomb lattice with abundant oxygen-containing functional groups, including for instance epoxy, hydroxyl and carboxyl groups[28]. Owing to the presence of these functional groups, GO sheets can easily be dispersed in water. Because of this, layered GO membranes can be easily prepared by using simple vacuum/pressure filtration[29,30], dip-coating[31], spin-coating[32] and rod-coating[33] methods. Using these methods, GO nanosheets can be layered into an interconnected nano-capillary structure. These nano-capillaries or nanochannels act as selective barriers which allow unimpeded water permeation while rejecting both impurities and salt ions[34,35]. Within these confined nanochannels, the unoxidised (or pristine graphene) regions provide a nearly frictionless region for transport of water, where the water molecules exhibit large slip length[36]. The structure of this interlayer gallery is crucial in determining the performance of layered GO membranes in separation and purification applications[37]. This struc-

[a] PLASMANT, Department of Chemistry, University of Antwerp, 2610 Antwerp, Belgium. E-mail: abhijit.gogoi@uantwerpen.be
[b] NANOlab Center of Excellence, University of Antwerp, Belgium.
[c] Department of Physics, University of Antwerp, 2020 Antwerp, Belgium.
[d] Departamento de Fisica, Caixa Postal 6030, Universidade Federal do Ceará, 60455-70 Fortaleza, Ceará, Brasil.

† Electronic Supplementary Information (ESI) available: LJ parameters and partial charges applied in the simulations, GO nanosheets and layered GO membrane, Water orientational relaxation dynamics for **RO+E** process, C(D) for layered GO membranes with **RO+E** process, C(D) for layered GO membranes for the Pure case, C(D) for layered GO membranes for the 3% case, C(D) for layered GO membranes for the 10% case, Diffusion of H_3O^+ ions, Diffusion of OH^- ions, Amount of functional groups on the reduced GO nanosheets, Water permeation events, Free energy barriers for the ions, Application of external pressure in the simulations, Application of constraints in the simulations. See DOI: 10.1039/b000000x/

ture can be altered for specific applications by controlling the degree of oxidation[38,39], size of the GO nanosheets, external pressure regulation[40], using crosslinkers[41] or by cationic intercalation to name a few. However, even after a decade of extensive research, real world applications of layered GO membranes are yet to be realized. One of the major challenges for the practical applicability of GO membranes is their inadequate stability in aqueous environment[42,43]. A number of strategies have been proposed to address this issue, including reduction of the GO nanosheets[44,45], the use of external cross-linkers[46,47], physical confinement of the GO layers[48,49], and cation intercalation[50–52]. In our previous work[1], we demonstrated that layered GO membranes can be stabilized in an aqueous environment by generating H_3O^+ and OH^- ions inside the interlayer gallery of the membrane. These ions form clusters in the interlayer gallery and act as physical binders between the GO nanosheets through hydrogen bonding (H-bonding). Apart from stabilizing the GO laminates, H_3O^+/OH^- clusters also increase the salt rejection of the membrane. However, the presence of these clusters also leads to a decrease in the water flux through the membrane, as compared to pristine layered GO membranes.

In this study, we propose a solution to this effect which involves the reduction of the GO nanosheets. The reduction of the GO nanosheets significantly increases the water flux of the GO membranes stabilized by the H_3O^+/OH^- ions, with very little changes (or no changes in some cases) in its selectivity. We performed large scale molecular dynamics (MD) simulations to obtain a detailed atomistic insight into the permeation processes through the GO membranes. The performance of these membranes is assessed for various degrees of reduction of the GO nanosheets. In the following sections, we explain the methodology adopted, present the results and discussion, and finally the conclusions drawn from this study.

2 Methodology

In this study, large scale MD simulations are performed to investigate the performance of layered GO membranes for various degrees of reduction. First, GO nanosheets are constructed using Visual Molecular Dynamics (VMD)[53] and Avogadro[54] software packages. The chemical composition of the GO nanosheet is $C_{10}O(OH)(COOH)_{0.5}$[55]. Hydroxyl and epoxy groups are located on the basal plane of the GO nanosheet while the carboxylic groups are located at the edges. The structure of the GO nanosheet is shown in Fig. S2a of the supporting information. In this study, 5 different degrees of reduction of the GO nanosheets are considered, viz. 0% (i.e., pristine GO), 10%, 30%, 50%, and 70% reduction. The reduced GO nanosheets are prepared by decreasing the number of oxygen containing functional groups on successive reduction. The amount of oxygen containing functional groups on the GO nanosheets corresponding to respective degree of reduction is reported in Table S3 of the supporting information. Layered GO membranes are then constructed using these nanosheets. The structural and geometric parameters of the membrane are provided in the supporting information (Fig. S2b). As reported in our previous study[1], we here also consider three different cases of water dissociation inside the interlayer gallery of layered GO membranes, viz. "Pure", "3%" and "10%". "Pure" refers to the case where no water molecule is dissociated inside the interlayer gallery. "3%" and "10%" refer to the cases where 3% and 10% of the water molecules, respectively, are dissociated into H_3O^+ and OH^- ions inside the interlayer gallery of the layered GO membranes. Before the construction of the simulation setup, membranes are hydrated with an equilibrated water box and the H_3O^+/OH^- ions are randomly placed inside the interlayer gallery of the membranes. These hydrated membranes are then equilibrated at 300 K and 1 atm pressure. To mimic the sea water osmotic pressure (about 27 atm), a 0.56 M aqueous NaCl solution is considered as the feed solution. This feed solution contains 10^4 water molecules, 108 Na^+ ions, and 108 Cl^- ions. The simulation setup is shown in Fig. 1. A transmembrane pressure (P) of 50 MPa is applied across the membrane using a graphene piston. As the water molecules can be dissociated into H_3O^+ and OH^- ions under the influence of external electric field[56], we consider the presence of an external electric field (E) along the direction of transmembrane pressure in our simulations. The oscillating AC electric field is given as $E = E_0 \cos(\omega t - \phi)$ where E_0 $\left(= 0.1 \frac{V}{Å}\right)$ is the amplitude, ω $\left(= 0.005\ \text{fs}^{-1}\right)$ is the frequency and ϕ $(= 90°)$ is the phase at the initial time step. On the permeate side, a fixed graphene sheet is placed which acts as a reservoir wall. We considered 2 different cases for the simulations. In the first case, simulations are performed only for the reverse osmosis (RO) process while in the second case, apart from RO, an external electric field is additionally considered along the direction of the transmembrane pressure (RO+E).

All MD simulations reported here are performed with NAMD 2.14[57] using the OPLS-AA force field parameters[58]. The water molecules are modeled with the SPC/E water model where the bond lengths of the water molecules are constrained using the SETTLE algorithm[59]. The van der Waals interactions are computed using a Lennard-Jones potential with a cut-off distance of 12.0 Å. For the computation of long range electrostatic interactions, the Particle mesh Ewald (PME) method[60] is used.

Before performing the production runs, the systems are first energy minimized and subsequently equilibrated for 2 ns at a constant temperature of 300 K and 1 atm pressure. Pressure is controlled using modified Nosé-Hoover method with a barostat oscillation time and damping factor of 0.3 ps. For controlling the temperature, Langevin dynamics is used with a damping factor of 5 ps^{-1}. After equilibration, the production runs are performed for 20 ns at a constant temperature of 300 K. During the course of the production runs, the interior GO nanosheets are constrained in the XY plane and are only allowed to move along the Z direction. The corner carbon atoms of the GO nanosheets at the top and bottom boundary of the membrane are fixed in space during the production run in order to clearly distinguish the membrane boundaries. Along the Z direction, a vacuum of 50 Å in length is applied on both sides of the simulated system. Periodic boundary conditions (PBC) are applied in all directions. For each simulated case, three independent simulations are performed with different initial configurations, and the results are averaged over these three independent simulations.

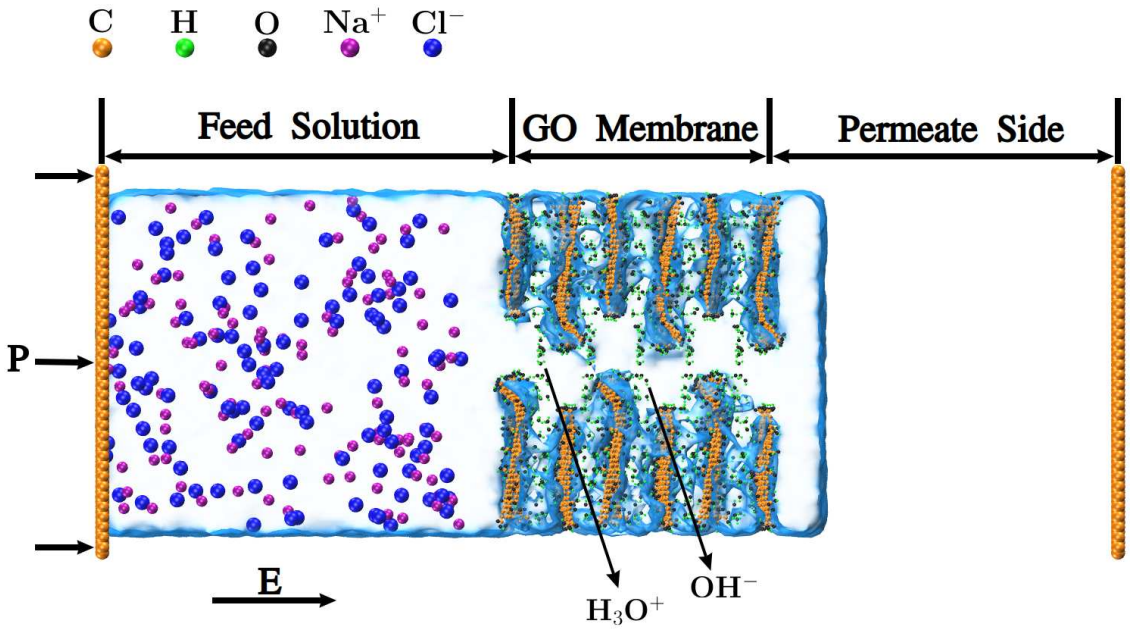

Fig. 1 Simulation setup. The feed solution is pressed through the layered GO membrane towards the permeate side with a transmembrane pressure P. An external electric field E is applied along the direction of the transmembrane pressure.

3 Results and discussion

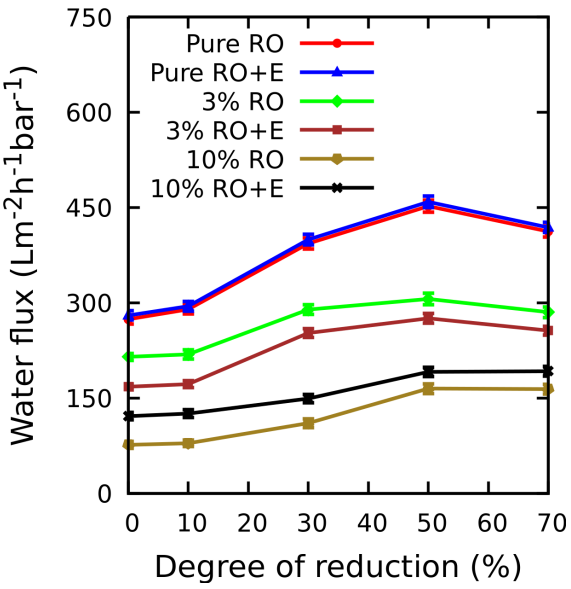

Fig. 2 Water flux through the layered GO membranes.

Typically, a good quality membrane should allow for a high water flux in combination with a high salt rejection. Fig. 2 shows the water flux through layered GO membranes for various degrees of reduction. As the water dissociation inside the interlayer gallery increases, the water permeance through the membrane decreases because of two reasons[1]: (a) formation of H_3O^+/OH^- clusters and (b) increased stability of the H-bond network between water molecules and GO nanosheets. In Fig. 2, it is observed that the water flux through the membranes increases as the degree of reduction of the GO nanosheets increases from 0 to 50 %. With a further increase in reduction, a decrease in the water flux is observed. This can be explained as follows. When the degree of reduction of the GO nanosheets initially increases, the layered GO membranes become more hydrophobic. Consequently, the H-bonding network between the water molecules and the GO nanosheets become less stable and water molecules permeate more easily through the membrane, thus increasing the water flux through the membrane. To compare the stability of the H-bonding network, we computed the following auto-correlation function[61,62]:

$$\mathbf{C(t)} = \frac{< \eta_{ij}(t)\eta_{ij}(0) >}{\eta_{ij}(0)^2} \cong exp\{-\frac{t}{\tau_i}\} \quad (1)$$

where

$$\eta_{ij}(t) = \begin{cases} 1 & \text{If there is a H bond between molecules i and j at times } 0 \text{ and } t \text{ and the bond has not been broken for any period longer than } t^* \\ 0 & \text{Otherwise} \end{cases}$$

The limiting cases $t^* = 0$ and $t^* = \infty$ correspond to the continuous ($\mathbf{C_C(t)}$) and intermittent ($\mathbf{C_I(t)}$) H-bond auto-correlation functions respectively. Considering the time scale and complexity of the simulated systems, we consider intermittent H-bond auto-correlation functions ($\mathbf{C_I(t)}$) in the present study. The lifetime of H-bonds (τ_i) between water molecules and GO nanosheets for different degrees of reduction of the GO nanosheets is shown in Fig. 3. For all cases of water dissociation considered (i.e. pure water, 3% dissociation and 10 % dissociation), the H-bonding network between the water molecules and the GO nanosheets becomes weaker with the reduction of the GO nanosheets. Con-

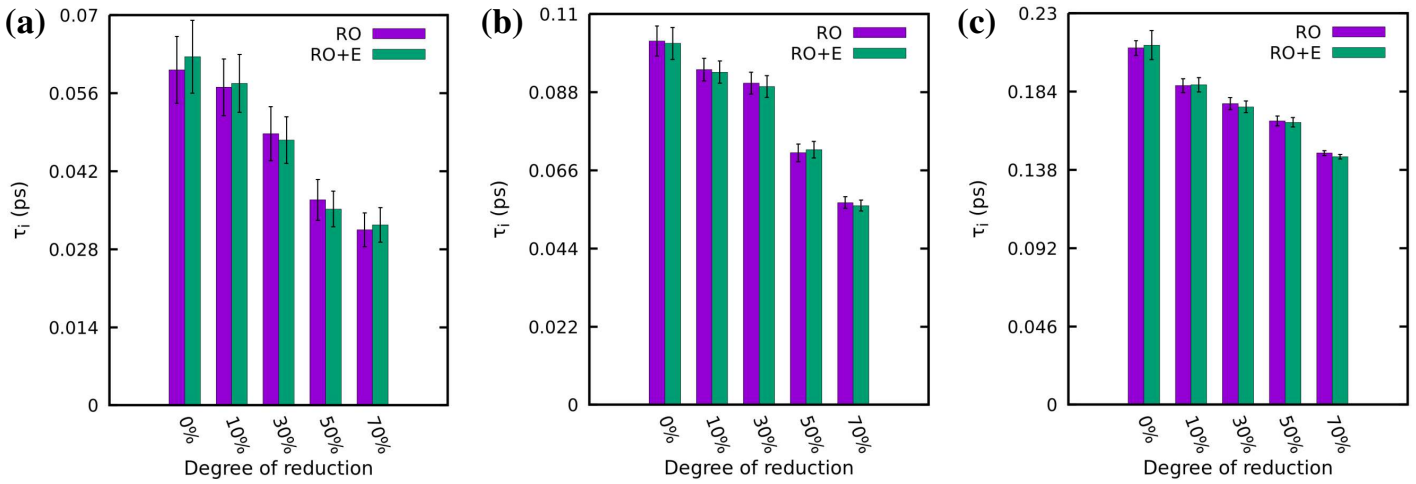

Fig. 3 H-bond lifetime between water molecules and GO nanosheets with different degree of reduction: (a) Pure, (b) 3% case, and (c) 10% case.

sequently, the water molecules can more easily permeate through the membranes, resulting in an increase in the water flux. In Fig. 3, it is also observed that with the increase in the dissociation of water molecules inside the interlayer gallery, the H-bonding network between the water molecules and the GO nanosheets becomes stronger. This is because of the clustering of H_3O^+/OH^- ions inside the interlayer gallery[1].

The decrease in stability of the H-bonding network between water molecules and GO nanosheets with the reduction of the GO nanosheets can be attributed to changes in the water orientational relaxation dynamics $\mathbf{C_e}$ inside the interlayer gallery. $\mathbf{C_e}$ can be calculated using the following auto-correlation function for the water dipole:[63,64]

$$\mathbf{C_e} =< L_2[\vec{u}(t_0)\cdot\vec{u}(t_0+t)] > \quad (2)$$

where, L_2 is the second-order Legendre polynomial and $\vec{u}$ is the unit vector along the dipole vector. A rapid decay of $\mathbf{C_e}$ indicates that water molecules are rapidly rotating, and vice versa. Fig. 4 shows the temporal evolution of $\mathbf{C_e}$ for the water molecules inside the interlayer gallery of layered GO membranes for the **RO** process. The value of $\mathbf{C_e}$ is 1 at time (t) = 0[63,64]. However, in Fig. 4, the value of $\mathbf{C_e}$ = 1 corresponding to t = 0 is not shown for better clarity. With an increase in the degree of reduction of the GO nanosheets, the water molecules inside the interlayer gallery tend to rotate more rapidly. Because of this increase in fluctuations, the H-bonding network between the water molecules and GO nanosheets becomes weaker. In Fig. 4, it is also observed that the temporal decay of $\mathbf{C_e}$ slows down with the increase in the dissociation of water molecules in the interlayer gallery. This can be attributed to the formation of clusters of H_3O^+/OH^- ions[1]. The temporal evolution of $\mathbf{C_e}$ for the **RO+E** process is reported in the supporting information (Fig. S3).

The reduction of the GO nanosheets and the clustering of the H_3O^+/OH^- ions also influences the structure of the layered GO membranes. To obtain a quantitative estimate, we computed a parameter C(D), using the method proposed by Bhattacharya and Gubbins[65], where C(D) represents the probability of finding a point inside the model structure with a pore size larger than or equal to D. Fig. 5 shows the C(D) for layered GO membranes in the RO process. As can be seen from this figure, pore sizes inside the interlayer gallery of layered GO membranes decrease with increase in the degree of reduction of the GO nanosheets. This is because of the decrease in the interlayer spacing between the GO laminates. Indeed, this will reduce the water permeance through the layered GO membranes. However, as observed in Fig. 2, water permeance increases as the GO nanosheets are reduced from 0 to 50%. Here, the decrease in the stability of H-bonding network between water molecules and GO nanosheets is the dominating factor over the decrease in the pore sizes. With further reduction of the GO nanosheets, the decrease in pore size of the membrane become the dominating factor over the instability of the H-bonding network. Consequently, the water flux through the layered GO membrane decreases as the GO nanosheets are reduced beyond 50% as observed in Fig. 2. However, this effect is less significant with the dissociation of water molecules inside the interlayer gallery of the membranes. C(D) for layered GO membranes for the **RO+E** process is reported in Fig. S4 of the supporting information.

Fig. 2 also shows the effect of the external electric field on the water permeance through the membranes. For the pure water case and the 10% water dissociation cases, the external electric field improves the water flux through the membranes, while for the 3% case, the water flux is seen to decrease. As reported in Fig. S5 of the supporting information, the pore size of the layered GO membrane increase for the pure water case with the application of external electric field. This can be attributed to the fluctuations of the GO nanosheets and directional motion of the ions under the influence of the external electric field[1]. Because of this increase in pore sizes, the water flux through the membrane increases. The influence of the external electric field for the 3% and 10% water dissociation cases are completely different. For the 3% case, the external electric field reduces the pore size of the membrane (Fig. S6), while for the 10% water dissociation case, the external electric field increases the pore size of the membrane (Fig. S7).

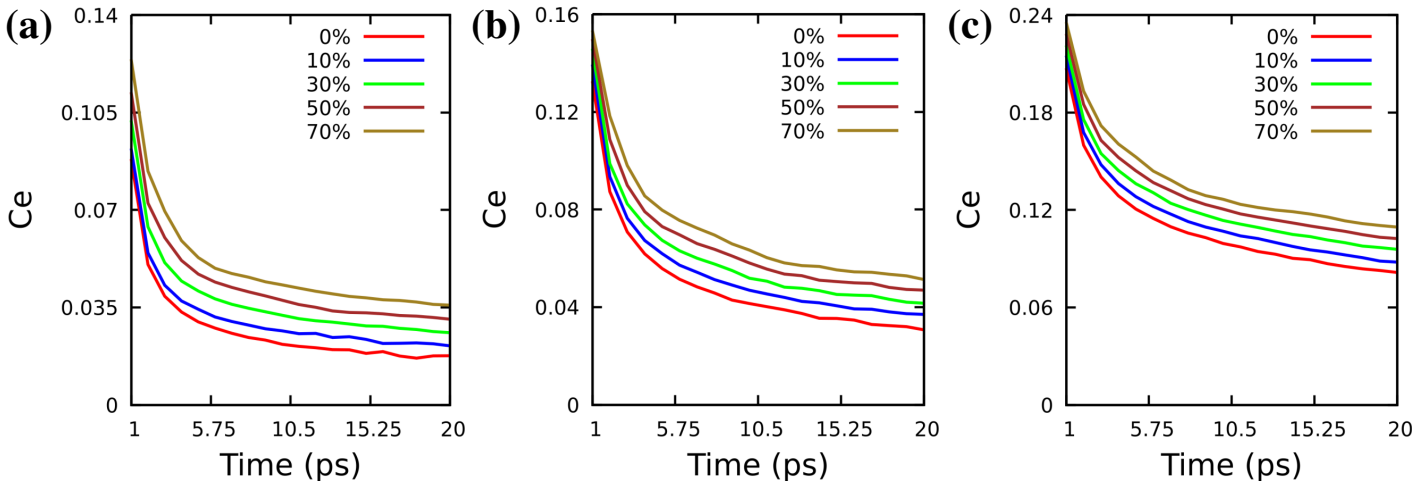

Fig. 4 Water orientational relaxation dynamics $\mathbf{C_e}$ inside the interlayer gallery of layered GO membranes for the **RO** process: (a) Pure, (b) 3% case, and (c) 10% case.

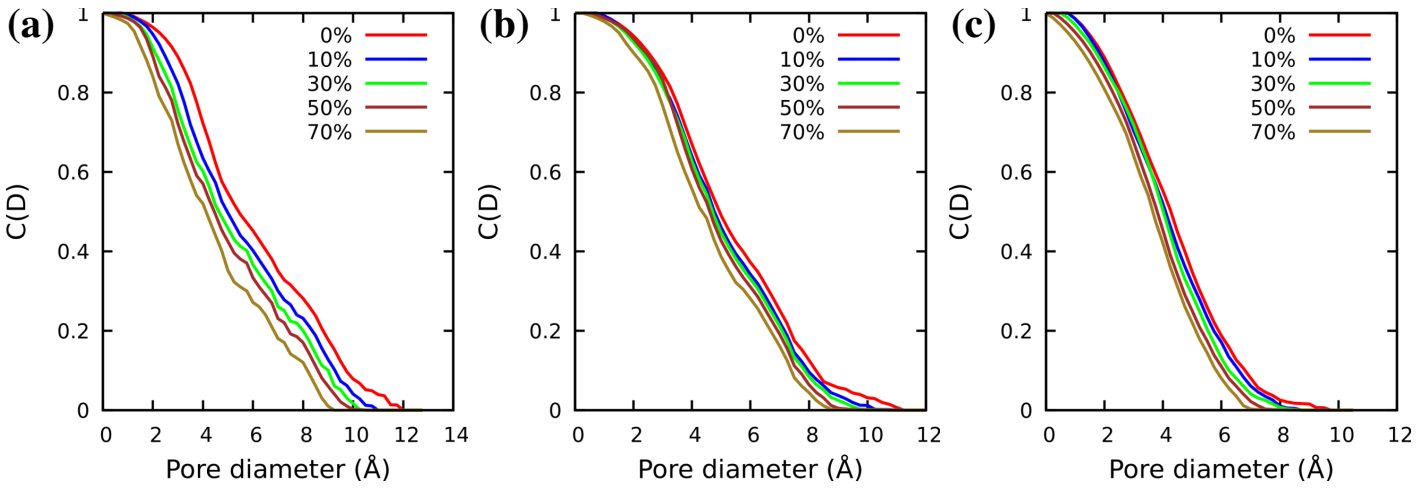

Fig. 5 C(D) for layered GO membranes for the **RO** process: (a) Pure, (b) 3% case, and (c) 10% case. C(D) represents the probability of finding a point inside the membrane with a pore size larger than or equal to D

This difference in the behaviour of electric field for the 3% and 10% water dissociation cases can be attributed to the diffusivity of the H_3O^+/OH^- ions under the influence of the external electric field[1]. As observed in Figs. S8 and S9, H_3O^+/OH^- ions become more diffusive under the influence of external electric field for the 3% case as compared to the 10% case. Because of this, the size of the H_3O^+/OH^- clusters reduce, which results in the decrease of the number of larger pores for the **RO+E** process as observed in Fig. S6. On the other hand, the effect of the external electric field on the diffusivity of H_3O^+/OH^- ions for the 10% case is almost negligible. This is because of the formation of larger clusters for the 10% water dissociation case which results in a more compact arrangement of H_3O^+/OH^- clusters inside the interlayer gallery. However, the pore sizes inside the interlayer gallery of layered GO membrane increase under the influence of external electric field for the 10% water dissociation cases (Fig. S7), due to the fluctuations of the GO nanosheets[1].

Apart from water flux, the ability of a membrane to reject impurities and ions is also very important in determining its performance. In our study, the salt rejection is calculated using the following formula

$$\text{Salt rejection} = \frac{\text{NI}_{\text{Feed}} - \text{NI}_{\text{Permeate}}}{\text{NI}_{\text{Feed}}} \times 100(\%) \qquad (3)$$

where NI_{Feed} is the number of ions in the feed solution and $\text{NI}_{\text{Permeate}}$ is the number of ions in the permeate side. In Fig. 6, we report the salt rejection of the layered GO membranes considered in this study. The dissociation of water molecules inside the interlayer gallery of layered GO membranes significantly improves the salt rejection of the membranes. For the pure water case, the external electric field reduces the Cl^- rejection while it increases the Na^+ rejection. This is because of the directional movement of the Cl^- and Na^+ ions under the influence of the external electric field. Also, the rejection of the Cl^- and Na^+

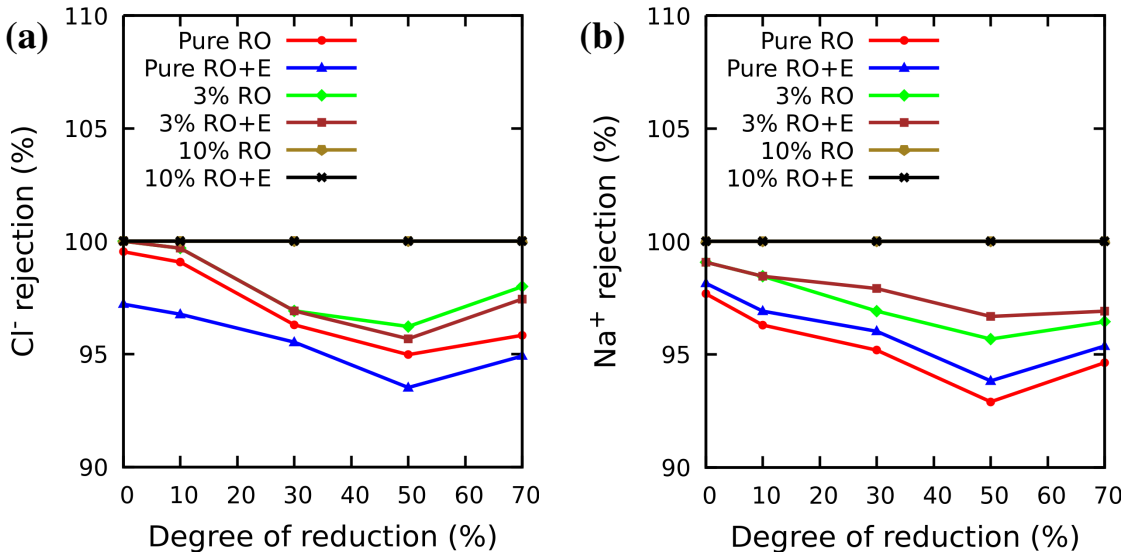

Fig. 6 Salt rejection of layered GO membranes: (a) Cl^- ion rejection, and (b) Na^+ ion rejection.

ions initially decreases with the reduction of GO nanosheets and then increases after 50% reduction. This is due to the correlated movement of these ions with the water flux. Cl^- and Na^+ ions move through the membrane as hydrated ions. Therefore, for the pure water case, the increase in the water flux also results in the decrease of the Cl^-/Na^+ rejection and vice versa.

For the case of 3% water dissociation, the external electric field has no effect on the Cl^- (Na^+) ion rejection up to 30% (10%) reduction of the GO nanosheets. This is because of the formation of H_3O^+/OH^- clusters inside the membrane. These clusters reduce the mobility of the Cl^-/Na^+ ions and hence their permeance through the membrane. However, with further reduction of the GO nanosheets, the decreasing stability of H-bonding network between water molecules and GO nanosheets become a dominant factor. Consequently, beyond 30% reduction, the rejection of Cl^- ion decreases with the application of external electric field (Fig. 6a). The electric field is applied along the direction of transmembrane pressure which favours the permeation of Cl^- ions through the membrane from feed side to permeate side. On the contrary, the electric field reduces the permeation of the Na^+ ions through the membrane from feed side to permeate side. Because of this, after 10% reduction, the rejection of Na^+ ions increases with the application of external electric field (Fig. 6b). For the case of 10% water dissociation, the H_3O^+/OH^- cluster sizes are much larger and hence, they are much more densely packed inside the interlayer gallery of layered GO membranes. Because of this, no Cl^- or Na^+ ion permeates through the layered GO membranes, i.e., 100% rejection of Cl^- and Na^+ ions is observed. This is an encouraging observation considering the typical tradeoff between water flux and salt rejection of a membrane. Indeed, in our study we observe an increase in the water flux of the membrane by reduction of the GO nanosheet (Fig. 2) without altering its selectivity (Fig. 6).

4 Conclusions

We performed large scale atomistic simulations in order to obtain detailed insights into the performance of layered GO membranes stabilized by H_3O^+/OH^- ions. A major issue for H_3O^+/OH^--stabilized layered GO membrane is the significant decrease in the water flux[1]. In this study, we showed that this problem can be resolved by reducing the GO nanosheets. Based on the parameters considered in this study, we observed that water flux through the layered GO membrane increases as the GO nanosheets are reduced from 0 to 50%. With further reduction of the GO nanosheets, the water flux decreases. Here, two factors are of importance. The first is the decrease in the stability of H-bonding network between water molecules and GO nanosheets, which contributes to an increase in the water flux. The second factor is the reduction in the pore sizes inside the interlayer gallery of the membrane, which results in a decrease in the water flux. For the initial reduction (0 to 50%) of the GO nanosheets the fist factor is dominant, effectively leading to an observed increased water flux through the membranes. With further reduction of the GO nanosheets (beyond 50%), the second factor becomes dominant, resulting in a decrease in the water flux. We also observed excellent salt rejection for all the membranes ($> 92\%$) considered in this study. In particular, for the case of 10% water dissociation, 100% salt rejection is observed for all studied cases. This is quite an encouraging observation considering that the water flux through the membrane can be increased without altering its selectivity. It would be interesting to further investigate the performance of these membranes with different feed solutions and with varying properties of the external electric field.

With regard to the observations reported in this study, one of the major challenges would be to dissociate water molecules into H_3O^+ and OH^- ions in a practical desalination system. On this note Zhou et al.[56], experimentally demonstrated the dissociation of water molecules into H_3O^+ and OH^- ions with the application

of an external electric field. However, to realized this in practical water purification and desalination units, more experimentation needs to be done. Another interesting aspect would be to investigate this separation process with forward osmosis (FO) which will eliminate the need of external transmembrane pressure and potentially be cost effective. In that regard, different combinations of draw and feed solutions could also be experimented.

Conflicts of interest

There are no conflicts to declare.

Acknowledgements

This work was supported by Research Foundation Flanders (FWO-Vl). The computational resources used in this work were provided by the VSC (Flemish Supercomputer Center), which is funded by Research Foundation Flanders and the Flemish Government department EWI.

Notes and references

1 A. Gogoi, E. C. Neyts, M. V. Milošević and F. M. Peeters, *ACS Appl. Mater. Interfaces*, 2022, **14**, 34946–34954.

2 D. I. Petukhov, O. O. Kapitanova, E. A. Eremina and E. A. Goodilin, *Mendeleev Commun.*, 2021, **31**, 137–148.

3 D. I. Petukhov, A. P. Chumakov, A. S. Kan, V. A. Lebedev, A. A. Eliseev, O. V. Konovalov and A. A. Eliseev, *Nanoscale*, 2019, **11**, 9980–9986.

4 O. Jankovský, D. Sedmidubský, P. Šimek, K. Klímová, D. Bouša, C. Boothroyd, A. Macková and Z. Sofer, *Phys. Chem. Chem. Phys.*, 2015, **17**, 25272–25277.

5 J. Liu, Z. Wang, L. Liu and W. Chen, *Phys. Chem. Chem. Phys.*, 2011, **13**, 13216–13221.

6 H. Zhao, L. Wu, Z. Zhou, L. Zhang and H. Chen, *Phys. Chem. Chem. Phys.*, 2013, **15**, 9084–9092.

7 A. Nicolaï, B. G. Sumpter and V. Meunier, *Phys. Chem. Chem. Phys.*, 2014, **16**, 8646–8654.

8 H. Gao, Q. Xu, J. Wang, C. Ning, Y. Liu, Y. Xie and R. Lu, *J. Phys. Chem. Lett.*, 2022, **13**, 258–266.

9 E. A. Chernova, D. I. Petukhov, A. P. Chumakov, A. V. Kirianova, I. S. Sadilov, O. O. Kapitanova, O. V. Boytsova, R. G. Valeev, S. V. Roth, A. A. Eliseev and A. A. Eliseev, *Carbon*, 2021, **183**, 404–414.

10 D. I. Petukhov, E. A. Chernova, O. O. Kapitanova, O. V. Boytsova, R. G. Valeev, A. P. Chumakov, O. V. Konovalov and A. A. Eliseev, *J. Membr. Sci.*, 2019, **577**, 184–194.

11 N. Raghav, S. Chakraborty and P. K. Maiti, *Phys. Chem. Chem. Phys.*, 2015, **17**, 20557–20562.

12 A. Y. S. Eng, C. K. Chua and M. Pumera, *Phys. Chem. Chem. Phys.*, 2016, **18**, 9673–9681.

13 Y. Li, D. Ye, B. Shi, W. Liu, R. Guo, H. Pei and J. Xie, *Phys. Chem. Chem. Phys.*, 2017, **19**, 7498–7505.

14 P. Malinský, A. Macková, R. Mikšová, H. Kováčiková, M. Cutroneo, J. Luxa, D. Bouša, B. Štrochová and Z. Sofer, *Phys. Chem. Chem. Phys.*, 2017, **19**, 10282–10291.

15 D.-H. Cho, W.-J. Lee, J.-H. Wi, W. S. Han, S. J. Yun, B. Shin and Y.-D. Chung, *Phys. Chem. Chem. Phys.*, 2018, **20**, 16193–16201.

16 J. A. Q. Renteria, C. Ruiz-Garcia, T. Sauvage, L. F. Chazaro-Ruiz, J. R. Rangel-Mendez and C. O. Ania, *Phys. Chem. Chem. Phys.*, 2020, **22**, 20732–20743.

17 A. Nordenström, A. Iakunkov, I. Baburin and A. Talyzin, *Phys. Chem. Chem. Phys.*, 2020, **22**, 21059–21067.

18 C. D. Williams, F. R. Siperstein and P. Carbone, *Nanoscale*, 2021, **13**, 13693–13702.

19 M. Neek-Amal, A. Lohrasebi, M. Mousaei, F. Shayeganfar, B. Radha and F. M. Peeters, *Appl. Phys. Lett.*, 2018, **113**, 119901.

20 S. E. Meragawi, A. Akbari, S. Hernandez, M. S. Mirshekarloo, D. Bhattacharyya, A. Tanksale and M. Majumder, *J. Mater. Chem. A*, 2020, **8**, 24800–24811.

21 S. Wang, D. Mahalingam, B. Sutisna and S. P. Nunes, *J. Mater. Chem. A*, 2019, **7**, 11673–11682.

22 L. Xie, L. Gong, J. Zhang, L. Han, L. Xiang, J. Chen, J. Liu, B. Yan and H. Zeng, *J. Mater. Chem. A*, 2019, **7**, 21944–21952.

23 W. Fei, M. Xue, H. Qiu and W. Guo, *Nanoscale*, 2019, **11**, 1313–1318.

24 T. M. McCoy, A. J. Armstrong, J. E. Moore, S. A. Holt, R. C. Tabor and A. F. Routh, *Phys. Chem. Chem. Phys.*, 2022, **24**, 797–806.

25 M. Z. Rahman, P. Maity, O. F. Mohammed and J. Gascon, *Phys. Chem. Chem. Phys.*, 2022, **24**, 11213–11221.

26 Z. Geng, W. Chen, Z. Qiu, H. Xu, D. Pan and S. Chen, *Phys. Chem. Chem. Phys.*, 2023, **25**, 9140–9151.

27 H. G. Kalashami, M. Neek-Amal and F. M. Peeters, *Phys. Rev. Mater.*, 2018, **2**, 074004.

28 W.-H. Zhang, M.-J. Yin, Q. Zhao, C.-G. Jin, N. Wang, S. Ji, C. L. Ritt, M. Elimelech and Q.-F. An, *Nat. Nanotechnol.*, 2021, **16**, 337–343.

29 B. Yuan, M. Wang, B. Wang, F. Yang, X. Quan, C. Y. Tang and Y. Dong, *Environ. Sci. Technol.*, 2020, **54**, 15442–15453.

30 J. Liu, N. Wang, L. J. Yu, A. Karton, W. Li, W. Zhang, F. Guo, L. Hou, Q. Cheng, L. Jiang, D. A. Weitz and Y. Zhao, *Nat. Commun.*, 2017, **8**, 1–9.

31 K. Goh, L. Setiawan, L. Wei, R. Si, A. G. Fane, R. Wang and Y. Chen, *J. Membr. Sci.*, 2015, **474**, 244–253.

32 R. R. Nair, H. A. Wu, P. N. Jayaram, I. V. Grigorieva and A. K. Geim, *Science*, 2012, **335**, 442–444.

33 Z. Liu, Z. Ma, B. Qian, A. Y. H. Chan, X. Wang, Y. Liu and J. H. Xin, *ACS Nano*, 2021, **15**, 15294–15305.

34 Y. Cao, Z. Xiong, F. Xia, G. V. Franks, L. Zu, X. Wang, Y. Hora, S. Mudie, Z. He, L. Qu, Y. Xing and D. Li, *Adv. Funct. Mater.*, 2022, **32**, 2201535.

35 M.-L. Liu, J.-L. Guo, S. Japip, T.-Z. Jia, D.-D. Shao, S. Zhang, W.-J. Li, J. Wang, X.-L. Cao and S.-P. Sun, *J. Mater. Chem. A*, 2019, **7**, 3170–3178.

36 F. Xu, Y. Song, M. Wei and Y. Wang, *The Journal of Physical Chemistry C*, 2018, **122**, 15772–15779.

37 L. Nie, K. Goh, Y. Wang, J. Lee, Y. Huang, H. E. Karahan, K. Zhou, M. D. Guiver and T.-H. Bae, *Sci. Adv.*, 2020, **6**,

eaaz9184.
38 Y. Wei, Y. Zhang, X. Gao, Z. Ma, X. Wang and C. Gao, *Carbon*, 2018, **139**, 964–981.
39 B. Qi, X. He, G. Zeng, Y. Pan, G. Li, G. Liu, Y. Zhang, W. Chen and Y. Sun, *Nat. Commun.*, 2017, **8**, 1–10.
40 W. Li, W. Wu and Z. Li, *ACS Nano*, 2018, **12**, 9309–9317.
41 T. Liu, L. Tian, N. Graham, B. Yang, W. Yu and K. Sun, *Environ. Sci. Technol.*, 2019, **53**, 11949–11959.
42 Y. Zhang, S. Zhang and T. S. Chung, *Environ. Sci. Technol.*, 2015, **49**, 10235–10242.
43 J. Ran, C. Chu, T. Pan, L. Ding, P. Cui, C.-F. Fu, C.-L. Zhang and T. Xu, *J. Mater. Chem. A*, 2019, **7**, 8085–8091.
44 Z. Zhao, S. Ni, X. Su, Y. Gao and X. Sun, *ACS Sustainable Chem. Eng.*, 2019, **7**, 14874–14882.
45 V. Strauss, M. Muni, A. Borenstein, B. Badamdorj, T. Heil, M. D. Kowal and R. Kaner, *Nanoscale*, 2019, **11**, 12712–12719.
46 L. Chen, L. Huang and J. Zhu, *Chem. Commun.*, 2014, **50**, 15944–15947.
47 Y. Song, R. Li, F. Pan, Z. He, H. Yang, Y. Li, L. Yang, M. Wang, H. Wang and Z. Jiang, *J. Mater. Chem. A*, 2019, **7**, 18642–18652.
48 J. Abraham, K. S. Vasu, C. D. Williams, K. Gopinadhan, Y. Su, C. T. Cherian, J. Dix, E. Prestat, S. J. Haigh, I. V. Grigorieva, P. Carbone, A. K. Geim and R. R. Nair, *Nat. Nanotechnol.*, 2017, **12**, 546–550.
49 W. Wu, J. Su, M. Jia, W. Zhong, Z. Li and W. Li, *J. Mater. Chem. A*, 2019, **7**, 13007–13011.
50 L. Chen, G. Shi, J. Shen, B. Peng, B. Zhang, Y. Wang, F. Bian, J. Wang, D. Li, Z. Qian, G. Xu, G. Liu, J. Zeng, L. Zhang, Y. Yang, G. Zhou, M. Wu, W. Jin, J. Li and H. Fang, *Nature*, 2017, **550**, 380–383.
51 Y. Yang, L. Mu, L. Chen, G. Shi and H. Fang, *Phys. Chem. Chem. Phys.*, 2019, **21**, 7623–7629.
52 S. Liang, S. Wang, L. Chen and H. Fang, *Sep. Purif. Technol.*, 2020, **241**, 116738.
53 W. Humphrey, A. Dalke and K. Schulten, *J. Mol. Graphics*, 1996, **14**, 33–38.
54 M. D. Hanwell, D. E. Curtis, D. C. Lonie, T. Vandermeersch, E. Zurek and G. R. Hutchison, *J. Cheminf.*, 2012, **4**, 1–17.
55 H. Tang, D. Liu, Y. Zhao, X. Yang, J. Lu and F. Cui, *J. Phys. Chem. C*, 2015, **119**, 26712–26718.
56 K.-G. Zhou, K. S. Vasu, C. T. Cherian, M. Neek-Amal, J. C. Zhang, H. G-Kalashami, O. P. M. K. Huang, V. G. Kravets, J. Abraham, Y. Su, A. N. Grigorenko, A. Pratt, A. K. Geim, F. M. Peeters, K. S. Novoselov and R. R. Nair, *Nature*, 2018, **559**, 236–240.
57 J. C. Phillips, R. Braun, W. Wang, J. Gumbart, E. Tajkhorshid, E. Villa, C. Chipot, R. D.Skeel, L. Kalé and K. Schulten, *J. Comput. Chem.*, 2005, **26**, 1781–1802.
58 W. L. Jorgensen, D. S. Maxwell and J. T. Rives, *J. Am. Chem. Soc.*, 1996, **118**, 11225–11236.
59 S. Miyamoto and P. A. Kollman, *J. Comput. Chem.*, 1992, **13**, 952–962.
60 U. Essmann, L. Perera, M. L. Berkowitz, T. Darden, H. Lee, and L. G. Pedersen, *J. Chem. Phys.*, 1995, **103**, 8577–8593.
61 D. C. Rapaport, *Mol. Phys.*, 1983, **50**, 1151–1162.
62 M. Matsumoto and K. E. Gubbins, *J. Chem. Phys.*, 1990, **93**, 1981–1994.
63 R. J. Mashl, S. Joseph, N. R. Aluru and E. Jakobsson, *Nano Lett.*, 2003, **3**, 589–592.
64 Y. L. Yeh and C. Y. Mou, *J. Phys. Chem. B*, 1999, **103**, 3699–3705.
65 S. Bhattacharya and K. E. Gubbins, *Langmuir*, 2006, **22**, 7726–7731.